Journal of Colloid and Interface Science **224,** 169–178 (2000)
doi:10.1006/jcis.1999.6687, available online at http://www.idealibrary.com on IDEAL®

Surface Properties of Vitreous Fibers

M. Francesca Ottaviani,*[,1] Maura Tomatis,† and Bice Fubini†

*Institute of Chemical Sciences, University of Urbino, Piazza Rinascimento 6, Urbino, Italy; and †Department of Chemistry IFM, University of Turin, Via P. Giuria 9, Turin, Italy

Received August 13, 1999; accepted December 13, 1999

The surface properties of various vitreous fibers, suspected to be toxic to humans and animals, were investigated by means of paramagnetic labels covalently linked to the surface. Computer-aided analysis of the electron paramagnetic resonance (EPR) spectra provided structural and dynamic information on the label and its environment. Calorimetric measurements provided information on the hydration mechanism. The results were analyzed in terms of (a) different polarity and interaction abilities of surface regions, (b) presence of ions at the surface, (c) silica contents, (d) vicinity of the interacting sites, (e) fiber dimension and morphology of the surfaces, and (f) water hydration. The mobility of the labels decreased due to interaction of the fibers with ions or ionic and polar groups at the surface. Close interacting sites were identified on the basis of spin–spin effects and were distinguished and quantified in strongly and weakly interacting sites. The spin-labeling technique indicated decreased ability of the surface to interact with decreased silicon concentration and in the presence of contaminants at the surface. The interaction with water revealed in all cases a substantial heterogeneity in hydrophilicity of surface sites. The labels were not easily hydrated. Vitreous fibers of various compositions adsorbed much more water than crystalline or amorphous silica; water coordinated to surface cations played a major role in the overall adsorption. The surface reaction mechanisms were the same on fibers of different compositions, but the surface composition affected the extent of adsorption. Glass wool exhibited a much higher adsorption capacity than rock wool under the same experimental conditions. In conclusion, the combination of EPR and calorimetric measurements provided insight into the surface properties of silica-based fibers.

Key Words: **fibers; labeled surface; EPR; calorimetry; surface properties.**

INTRODUCTION

Fibrous and nonfibrous silica-based particles are extensively used in several industrial processes. Surface reactivity plays a fundamental role in most of these processes. Furthermore, silica-based fibers, widely used as asbestos substitutes, are known or suspected to be highly pathogenic to the respiratory system when inhaled (1–3). It is generally agreed that the surface properties of the particles determine the pathogenic mechanisms (4–7). Different surface functions, mainly silanols, siloxanes, dangling bonds, and transition metal ions, may be involved at different stages of the pathogenic process (8). Knowledge of the surface properties of the particles, mainly of their surface reactivity, is hence of paramount relevance in the industrial, environmental, and toxicological fields (4–7).

Most real surfaces being heterogeneous in nature, their reactivity is determined by the type and distribution of various surface groups and by micromorphology at the atomic level. Particles with the same chemical composition and crystalline structure have often been found to elicit different biological responses (2–4, 8, 9). These differences are likely due to small variations in surface properties which are rather difficult to evidence. In this respect stable radicals (spin labels or spin probes) are suitable for investigating small variations in the microtopography of the surface they are sitting on (10, 11). The computer-aided analysis of electron paramagnetic resonance (EPR) spectra of spin labels attached to surfaces has been successfully employed to provide structural and dynamic information on different surface functions and their environment and to monitor interactions between particles and cells (12, 13).

The present paper reports several kinds of information on the state of the surface, obtained by linking a spin label (a stable nitroxide) to the surface of silica-based fibers. The aim of the research was to investigate surface characteristics of artificial fibers (mainly glass and rock wool) used as standard samples for *in vitro* and *in vivo* toxicity tests. Most artificial fibers—used as asbestos substitutes, whether glassy or ceramic—are made up of mixtures of oxides, among which silica is a major component. The artificial fibers used in the present study were selected on the basis of their silica content and of their fiber shape and dimensions to investigate the effect of these properties on their surface reactivity. Table 1 reports the composition in oxides (percentage in weight) of the fibers (MMVF = man-made vitreous fiber; JM = from Johns–Manville Co.), obtained as described in Ref. (14); only percentages above 0.5% are reported.

The Si–OH groups at the surface were attached to an aminopropyltrimethoxysilane group onto which a nitroxide group was covalently linked. The labeling ability of different surfaces may thus be considered a measure of the surface reactivity toward reagents to be linked to surface silicon groups. Under these

[1] To whom correspondence should be addressed.

0021-9797/00 $35.00

TABLE 1
Composition in Oxides (Percentage in Weight) of the Fibers

%	JM104	MMVF10	MMVF11	MMVF21	MMVF22
SiO_2	62–65	57–58	63–64	46–47	38–39
Al_2O_3	3–5	5–6	4–5	13–14	10–11
B_2O_3	5–6	8–9	4–5	—	—
K_2O	0–1	1–2	1–2	1–2	—
Na_2O	14–16	15–16	15–16	2–3	—
MgO	2–3	4–5	2–3	9–10	10–11
CaO	5–6	7–8	7–8	17–18	37–38
TiO_2	—	—	—	2–3	—
Fe_2O_3	—	—	—	7–8	—

Note. (MMVF = Man-Made Vitreous Fiber; JM = from Johns-Manville Co.); only percentages above 0.5% are reported.

circumstances the spin-labeling technique may thus be employed to evaluate the distribution of silicon atoms at the surface. The feature of the EPR spectrum recorded depends on the atoms or ions surrounding the linking site; thus, the local topography of the surface on silica-based fibers was monitored.

The heat of adsorption of water as well as the adsorption isotherms was measured on some of the vitreous fibers to evaluate the overall reactivity of the fibers and the degree of hydration as functions of the partial pressure of water. Spin-labeled fibers were then dosed with water up to well-defined hydration states to investigate whether labeling preferentially occurs on hydrophilic or hydrophobic patches.

MATERIALS AND METHODS

Materials

The four glass and rock fibers employed—termed MMVF (Table 1 shows the composition, obtained as described in Ref. (14a))—were from the Thermal Insulation Manufacturers Association (TIMA) fiber repository, namely, MMVF10 and MMVF11 (both glass wool) and MMVF21 and MMVF22 (both rock wool), and were kindly provided by the Joint European Medical Research Board (JEMRB) from different preparation lots, as used in the Research and Consulting Co. (RCC) studies (14b). They were used as received. One short fiber sample, JM104 (Table 1 reports the composition, obtained as described in Ref. (14a)), was from Johns–Manville Co. and differed from the MMVFs mainly in fiber shape and size and preparation route (slow cooling from the melt instead of quenching). The physicochemical properties of the fibers were also obtained as described in Ref. (14a), such as the size, which was evaluated by SEM. Both calorimetric and EPR data are completely reproducible for repeated measurements on different and newly prepared samples under various experimental conditions.

Labeling Procedure

Several labeling methods have been reported in the literature (15–17). As one of the goals of the research was the preparation of labeled fibers to be used in biological media (12), we adopted the labeling procedure reported by Hall and Waterton, which yields covalent-bonded chains stable in aqueous media (12, 13). Scheme 1 shows the labeling procedure, which is as follows: the fibers were washed thoroughly with dilute hydrochloric acid and then with doubly distilled water to remove contaminants and traces of iron. Then, 0.5 g of the fibers was first silanized by the adsorption of 5 ml of freshly hydrolyzed 3-aminopropyltrimethoxysilane (Sigma, used as received, termed AMPTS, final concentration 10% (v/v)) from degassed aqueous alkaline solution (carbonate buffer at pH 9.2, corresponding to a concentration of 0.54 M). After equilibration under stirring for 24 h, filtration, and water washing, drying in an oven (50°C) improves the covalent fixing of the propylamine chain to the surface at the SiOH sites. Furthermore, at the alkaline pH used for the silanization, the amino group of silane is unprotonated and hydrolysis produces oligomers which easily react with the silicic surface. In this condition AMPTS forms an intramolecolar 7-ring. However, we cannot exclude a partial polymerization of AMPTS at the surface, at low relative percentage, but the silane layers over the covalently bonded layer are very weakly interacting with the surface and are easily removed by washing. Indeed, washing and drying of the fibers after

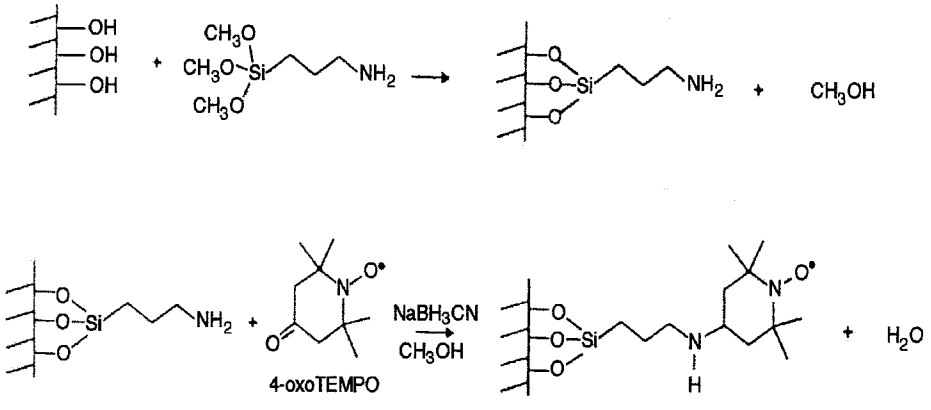

SCHEME 1

equilibration with the silanol solution have the capacity to stabilize the covalent binding of silanols and remove the physisorbed molecules.

Silanized surfaces were spin labeled by reductive amination using different concentrations of 2,2,6,6-tetramethyl-4-oxopiperidine-1-oxyl (TEMPO, Sigma, used as received) with an excess of sodium cyanoborohydride ($NaBH_3CN$, Sigma, used as received) as the reductant in methanol for 24 h (17). The unreacted material was removed by repeated water washing. The fibers were finally dried under vacuum. First, we performed an analysis of the labeling as a function of the label concentration. A progressive line-broadening of the EPR features followed by a collapse of the hyperfine lines into a single broad line was found, as expected for the increasing local concentration of labels at the surface. Then, two different TEMPO concentrations were selected: 5 and 50 mM. The lower one (low local surface concentration of labels) yields EPR spectra where the hyperfine splitting components are well detectable; the higher one is employed to fully saturate the functionalized surface and yields broad, unresolved EPR spectra. The 50 mM solution ensures the complete labeling of the surface, and in spite of the broad single line, it allows better comparison and differentiation among the samples (see below).

Contact of the Samples with Water Vapor

The sample, placed either in a calorimetric cell (heat of adsorption) or in an EPR cell (partial hydration of labeled fibers), was dosed with water vapor. Both cells were vacuum-tight and connected to a volumetric dosing vacuum frame. Gas-free water vapor was obtained by subsequent distillation and thawing in vacuum.

Methods

EPR spectra were recorded with a Varian E109-EPR spectrometer, working in the X band (about 9.5 GHz) with a double resonant cavity or with an Adani PS100-X EPR spectrometer, or with a Bruker 200D spectrometer, operating in the X band, interfaced with Stelar software to a PC-IBM computer for data acquisition and handling. The temperature was controlled with the aid of a Bruker ST 100/700 variable-temperature assembly. Magnetic parameters were measured by field calibration with the 1,1-diphenyl-2-picryl hydrazine (DPPH) radical ($g = 2.0036$).

The EPR measurements were performed at 298 K (303 K, as used in the calorimetric measurements, produced faster degradation of the radical, but no significant spectral variations were found between 298 and 303 K).

The heat of adsorption was determined by means of a Tian-Calvet microcalorimeter (Setaram) connected to a volumetric apparatus which allowed simultaneous measurement of the amount adsorbed (uptake, n_a), heat released (Q), and equilibrium pressure (p) for small increments of water vapor with which the sample was dosed. The procedure has been thoroughly described in previous papers (18). Before the adsorption of water vapor, each sample was degassed for 2 h at 150°C to remove physisorbed water. The temperature of the calorimeter was maintained at 30°C throughout the adsorption experiment. A typical adsorption sequence comprised two runs, with the following procedure: (i) dosing the sample with successive amounts of water vapor up to a pressure of typically 5–10 Torr (Ads I), (ii) desorption under vacuum, and (iii) readsorption of doses to evaluate the reversible adsorption (Ads II).

RESULTS AND DISCUSSION

Analysis of the EPR Spectra

The spectra were computed by means of the well-established procedure of Schneider and Freed (19). The principal informative parameters extracted from computation were as follows:

(a) The components of the **A** tensor for the hyperfine coupling between the nuclear spin and the electron spin. We used the components reported in Ref. (13) for silica-labeled particles: A_{xx}, A_{yy}, $A_{zz} = 7.0$, 7.0, 37.0 G. These components are diagnostic of a polar environment of the radical. A decrease in environmental polarity corresponds to a decrease in A_{ii} values.

(b) The correlation time for the rotational diffusion motion, τ_c (19). The accuracy in the evaluation of this parameter (usually 5%) strongly diminishes in the case of spin–spin-broadened or exchange-narrowed signals.

(c) The intrinsic linewidth $1/T_{2.0}$, indicated as ΔH and measured in gauss, which includes spin–spin relaxation effects (20, 21). The evaluation of the dipolar broadening (due to anisotropic spin–spin interactions), ΔH_D, by means of spectral computation allows one to calculate the mean distance, d (in angstroms), among the probes at the surface from the equation (22)

$$\Delta H_D = 3 \times 10^4 / d^3. \quad [1]$$

(d) The Heisenberg spin–spin-exchange frequency, ω_{ex}. The increase in ω_{ex} also corresponds to the increase in the local concentration of the radicals, which collide during their motion in nonviscous media. The relaxation rates due to the spin-exchange mechanism (T_{2E}^{-1}) linearly depend on the radical concentration (M),

$$T_{2E}^{-1} = K_E M, \quad [2]$$

where K_E is the second-order rate constant for the exchange process.

From the relationship between the linewidth and the spin state lifetime, a proportionality between the exchange frequency and the local concentration of radicals is established: $\omega_{ex} \propto M_{loc}$.

The linewidth decreases with increasing temperature for the Heisemberg spin-exchange mechanism, whereas the linewidth increases with increasing temperature when the dipolar interaction prevails (23).

Radicals in two different environments and in slow exchange in the EPR time scale generated different EPR signals that

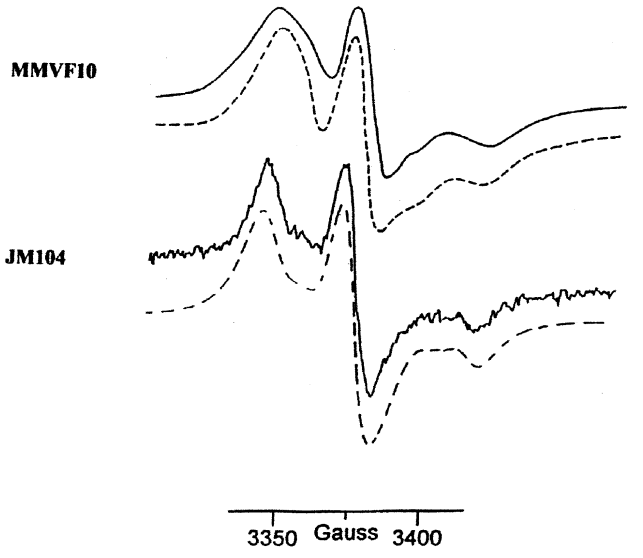

FIG. 1. EPR spectra of labeled MMVF10 and JM104. Full lines, experimental spectra; dashed lines, computed spectra (main parameters in Table 2). The labeling was obtained from a 5 mM solution of nitroxide.

superimposed to form the overall EPR spectra. The analysis of these spectra by means of a subtraction–addition procedure of experimental and computed components allowed evaluation of the partitioning of the radicals in the different environments.

The double integration of the adsorption signals allowed us to roughly compare the intensities of the EPR signals from different samples in the same experimental conditions. Henceforth, the intensities of the EPR signals are indicated as low, middle, high, and very high.

Of course, the reliability of the parameters was ensured by the reproducibility of the spectra in repeated experiments carried out for different preparations of the samples.

Characterization of the Surface Properties of Fibers by Means of the Spin-Labeling Technique

Figure 1 compares the EPR spectra of labeled MMVF10 and JM104. The full lines are the experimental spectra, and the dashed lines are the spectra computed with the main parameters reported in Table 2. The labeling was obtained on all samples from a 5 mM solution of nitroxide. Spectra from the other fibers are not reported since they are not informative for the purposes of the present study. The comparison between MMVF10 and JM104 is particularly interesting because the silica content is almost equivalent for the two fibers (about 60% in SiO_2—see Table 1), but the former has a diameter of 6 μm whereas the latter has a diameter of 0.1 μm. The two spectra differ (a) in the relative intensity, that of JM104 being much lower than that of the spectrum of MMVF10; (b) in label mobility, τ_c being higher (lower mobility) for the labels at the JM104 surface than that for the labels at the MMVF10 surface; (c) in spin–spin interactions, weaker (lower ΔH) for the labels at the JM104 surface than for the labels at the MMVF10 surface; and (d) in a second minor component (15%) characterized by quite high mobility, only present in the EPR spectrum of MMVF10. All these findings indicate the following: (i) the JM104 surface has a labeling ability lower than that of MMVF10, mainly due to few adjacent Si–OH groups available for labeling; (ii) the labels are far from one another at the JM104 surface, each label being free to interact with neighboring groups and ions at the surface with, as a consequence, hindered mobility of the labels. The preparation procedure for JM104 involves a lower density of silicon atoms, hence of silanols, at the surface. Also, the small diameter of the JM104 fibers may be responsible for the low interacting ability. The small (15%) fraction of labels in higher mobility conditions at the MMVF10 surface is probably localized in a less hydrophilic region (for instance, in the vicinity of Si–O–Si bridges). Therefore, the interactions of the labels with neighboring groups at the surface is weak.

The general composition of MMVFs and particularly the silica percentage vary, as shown in Table 1. Various lots of MMVFs were obtained from TIMA, and they were all processed as received, by means of the spin-labeling technique, to investigate their surface reactivity. Discrepancies within different lots of the same fiber type would testify to surface contamination. The labeling of all the MMVFs considered from lot 1 (the other lots tested in this work, excluding the lot indicated as lot 2, provided the same type of spectra as lot 1 and are not henceforth discussed), with a radical concentration of 50 mM, produces the series of EPR spectra shown in Fig. 2A: (a) MMVF10, (b) MMVF11, (c) MMVF20, (d) MMVF21. The full lines are the experimental spectra consisting of a broad single line. The dashed lines are the spectra computed with the main parameters listed in Table 3. Calculation on the basis of the surface area and Si–OH–groups distribution indicated that a 1.5 mM solution of

TABLE 2
Relevant Parameters Obtained from the Analysis of the EPR Spectra of Labeled Fibers

Silicate	τ_c ($\times 10^{-9}$ s)	ΔH (G)	Relative intensity
JM104	20.0	5.0	Low
MMVF10[a]	7.0	8.0	High

[a] 85% of the labels (from double integration of the signal components obtained from computation of the EPR lineshape). The remaining 15% of the labels show fast motion ($\tau_c \approx 5 \times 10^{-10}$ s).

TABLE 3
Relevant Parameters Obtained from the Computation of the EPR Spectra of MMVFs

Fiber	τ_c ($\times 10^{-9}$ s)	ΔH (G)	ω_{ex} ($\times 10^8$ s^{-1})
MMVF10 (lots 1–2)	(7)	2	4.0
MMVF11 (lot 1)	7	13	0.7
MMVF11 (lot 2)	(7)	2	4.0
MMVF21 (lots 1–2)	(7)	4	3.0
MMVF22 (lots 1–2)	7	18	1.0

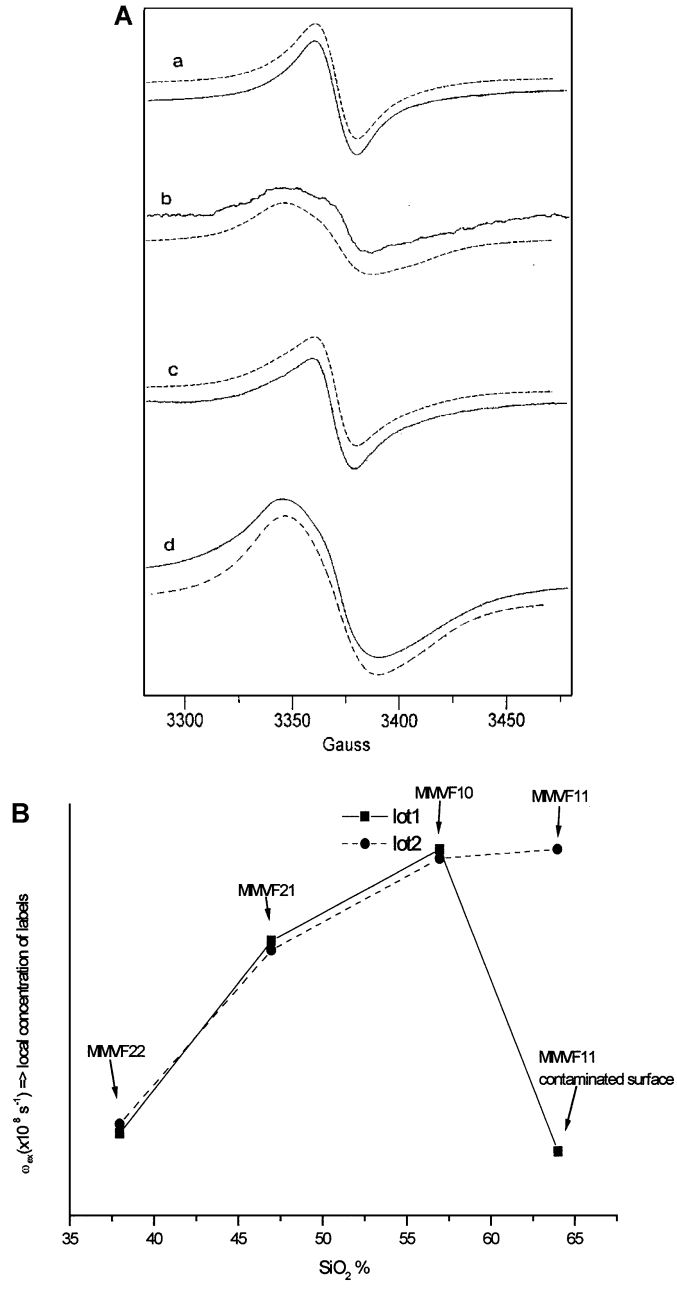

FIG. 2. (A) EPR spectra obtained from labeled MMVF fibers from lot 1 (radical concentration for labeling, 50 mM): (a) MMVF10; (b) MMVF11; (c) MMVF20; (d) MMVF21. Full lines, experimental spectra; dashed lines, computed spectra (main parameters in Table 3). (B) Exchange frequency, ω_{ex}, evaluated from the analysis of the spectra in A, as a function of the percentage of silica of the four MMVFs of lot 1 (full circles, superimposed onto full squares for MMVF22, MMVF21, and MMVF10) and lot 2 (full squares).

the nitroxide is needed to completely label the silica groups of 0.5 g (the starting amount used for the labeling procedure) of MMVF10 or MMVF11. But lineshape invariance was only obtained at [nitroxide] > 20 mM. This means that an excess of the radical in solution (at least 10 times higher concentration) was requested to guarantee complete labeling of the surface. Therefore, we selected a 50 mM solution to ensure complete labeling of the surface. The radicals which remained in solution or were physisorbed by the surface at the end of the labeling procedure were washed out. Such high labeling is responsible for the collapse of the hyperfine lines into a single line arising from strong spin–spin interactions. Both the dipolar broadening (increase in $1/T_{2,0}$) and the increase in the exchange frequency (increase in ω_{ex}) indicate a remarkable increase in the local concentration of the labels. The dipolar broadening arises from the radicals rigidly fixed at the surface. Only above "saturation" of the most interacting silica sites at the surface did further linking of the radicals lead to dynamical spin–spin interactions (Heisenberg spin–spin-exchange mechanism), which is responsible for the spectral feature (broad single line) in Fig. 2. This feature diminishes the accuracy in the evaluation of the correlation time for motion—evidently under slow motion conditions—which is, therefore, reported in parentheses. Such unresolved spectra were more informative than the narrow ones with respect to comparison and differentiation among the various samples. Since the labels were attached to surface silicon groups, the exchange frequency, corresponding to the local concentration of the spin labels, should increase with increased silica content of the fiber. The plot of ω_{ex} ($\propto$ local concentration) as a function of the percentage of silica is shown in Fig. 2B for the four MMVFs of lot 1 (full circles, superimposed on to full squares for MMVF22, MMVF21, and MMVF10) and lot 2 (full squares). Even if not in a linear fashion, the surface concentration of the labels increases with the increase in the nominal silica content of the fibers (for MMVFs, the surface reflects the composition of the bulk). The results from the two lots were coincident (the same values) for MMVF21, MMVF22, and MMVF10, whereas ω_{ex} from lot 1 of MMVF11 was well below the value found for lot 2. A chemical analysis of MMVF11 fibers from lot 1 indicated the presence of contaminants (various organic molecules). These strongly bound organic molecules prevent the spin-labeling of the surface itself. Our procedure could thus be regarded as a precise way to evidence surface contamination. Removing the contaminants by thorough washing of the fibers with strong acids reproduces the spectrum of MMVF11 from lot 1. The reproducibility of the results among different lots, the strongly contaminated ones being washed with strong acids and the "natural" ones (poorly contaminated) being washed with weak acids, ensures that washing with acids does not modify the surface properties. Indeed, it is reported in the literature (14) that the fibers used in the present study are well resistant (not dissolved or surface modified) to the acid treatment. By extrapolation of the ω_{ex} vs silica plot (Fig. 2B) to $\omega_{ex} = 0$, we obtain about 30% of SiO_2. This condition corresponds to the presence of labels only on the rigid, most strongly interacting sites, at which the dipolar broadening reached its maximum value. Of course, this result is significant only if we assume that the labeling abilities of the different MMVFs are equivalent. The increase in ω_{ex} was not linear with the increase in the silica content, but become almost constant for $SiO_2 > 60\%$. This indicates a "saturation"

condition of the weakly interacting sites, at which the labels retained high mobility. These results are complementary to the data obtained in the previous section for labeled MMVF10. Two components clearly contribute to the overall lineshape. The minor component (15%) showed faster mobility, which indicated that a portion of the interacting sites (weakly interacting sites) gave more mobile labels. A previous study also supported this finding (13). The present analysis indicates that the first sites which were labeled were the strongly interacting sites. After they were saturated, the weakly interacting sites were progressively occupied and saturated. Equation [1] allows evaluation of the mean distance—*d*—among the labels at the strongly interacting sites (dipolar interaction): for MMVF22, we obtained $d = 12.5$ Å. When the weakly interacting sites were progressively occupied, the Heisenberg exchange interaction (collisions among locally concentrated radicals not rigidly fixed at the surface) prevails, and Eq. [1] is no longer valid. It is noteworthy that the computation of the MMVF10 signal was performed with ΔH (linewidth) = 8 G (Table 2) for the starting 5 mM label solution, whereas $\Delta H = 2$ G (Table 3) was used for the starting 50 mM solution. This decrease in linewidth may be ascribed to the saturation of the strongly interacting sites. At 5 mM almost all the labels are strongly interacting with the surface (low mobility) and spin–spin interactions are mainly dipolar (also tested by the increase in ΔH by increasing temperature). In contrast, with a 50 mM solution, most labels are weakly interacting and faster moving; the collisions among both the strongly and the weakly interacting labels decrease the dipolar interactions and increase the exchange frequency (Heisenberg dynamic spin–spin interactions).

Surface Reactivity toward Water

The fibers were exposed to water vapor. In most cases, an exposition of more than 12 h was necessary to detect any change in lineshape. This indicates that water is initially attracted by surface sites not in proximity to the labels. Dosing of the surfaces of labeled fibers with water vapor was followed in two ways:

—subsequent doses and measure of the relevant EPR spectrum;

—contact of the labeled fiber with the vapor pressure and registration of the EPR spectrum at subsequent time points.

In the first case the EPR spectrum, typical of a label strongly linked to the surface and interacting with neighboring labels, did not change until the saturation vapor pressure was attained. In the second case the spectrum evolved toward that typical of the mobile label only after exposure of the fibers to vapor for several hours. The label on MMVF21 was more easily hydrated than that on MMVF11 (figures not reported for the sake of brevity). The same experiment done with *tert*-butanol reveals that, in contrast to water, the alcohol is not capable of overcoming the strong interaction of the label with the other labels, as no changes are visible, even after long periods of contact with the vapor.

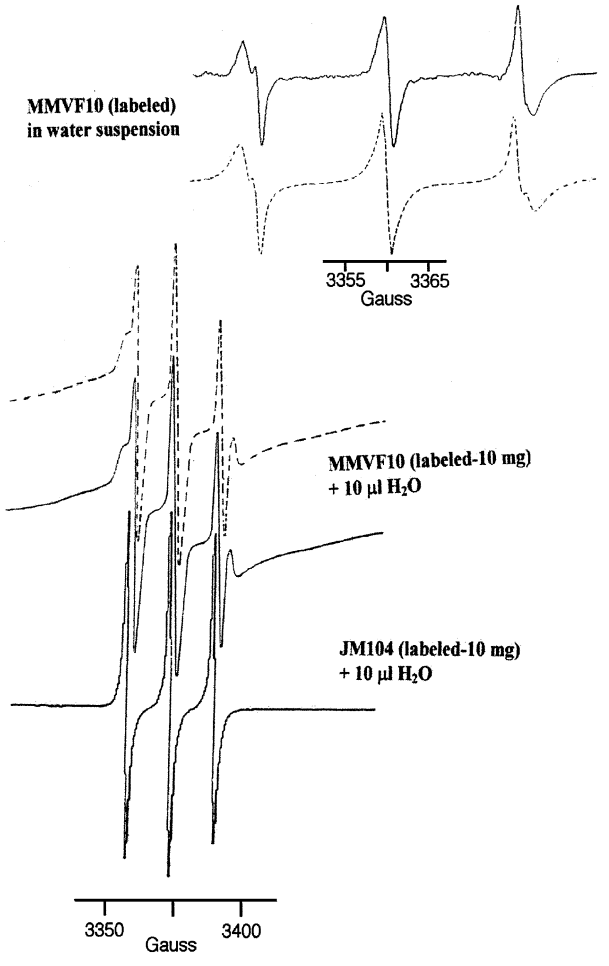

FIG. 3. Representative EPR spectra obtained for labeled vitreous fibers under various hydration conditions: JM104 and MMVF10 + 10 μL of water; MMVF10 in a water suspension. Full lines, experimental spectra; dashed lines, computed spectra (main parameters in Table 4).

Both experiments indicate that the label is strongly interacting via polar or H-bonding to the other labels. Much water is adsorbed without interference with the label.

Figure 3 shows representative EPR spectra obtained for vitreous fibers in various hydration conditions. If the labels are not detached from the surface by water, as usually happens to our samples, reversibility conditions are ensured by the reproducibility of the EPR signals upon subsequent drying and wetting processes. This also guarantees the persistency of the covalent labeling. The spectra of labeled JM104 and MMVF10 were recorded after addition of 10 μL of water. The spectrum of labeled MMVF10 in a water suspension is also shown. The full lines are the experimental spectra, and the dashed lines are the spectra computed with the parameters reported in Table 4. "Polar" in Table 4 corresponds to $A_{ii} = 7.0, 7.0, 37$ G, whereas "low polar" corresponds to $A_{ii} = 5.0, 6.0, 35$ G, and they indicate a polar and low-polar environment of the radicals, respectively. The polar environment mainly arises from water molecules in the vicinity of the N–O groups or ions at the

TABLE 4
Main Parameters Obtained from Computation of the EPR Spectra of Labeled Fibers under Different Hydration Conditions

Fiber	Water	Environment	τ_c ($\times 10^{-10}$ s)	ΔH (G)	%
MMVF10	10 μL	polar	70	14[a]	60
		low-polar	0.8	1.0	30
		polar	3	3.5	10
MMVF10	Suspension	polar	1	3.5	70
		low-polar	0.1	0.5	30
JM104	10 μL	low-polar	0.1	0.5	100

[a] $\omega_{ex} = 1 \times 10^8$ s.

surface (for the type of cations, see Table 1). The low-polar environment mainly arises from low-polar surface groups (Si–O–Si groups, for instance, which are not labeled, the labels may direct their N–O groups in the direction of these low-polar surface sites) + propyltrimethoxysilane + organic contaminants. Of course, water will participate in the hydration layer of the nitroxide group in both cases, but we have to take into account the partial hydrophobicity of both the solid surface (Si–O–Si groups) and the TEMPO–aminopropyltrimethoxysilane group. Therefore, a competition takes place for the interaction of water and other polar molecules with the surface and the nitroxide group. When the hydrophobic character of the label prevails, the surface hydration is favored at hydrophilic sites located far from the labels. This indicates the hydrophobic character of the surface regions which host the labels.

The following information is drawn from the analysis of the spectra in Fig. 3 and the corresponding parameters in Table 4:

(1) On MMVF10, unexpectedly, after addition of 10 μL of water, 60% of the labels were still slow moving and also retained strong spin–spin interactions (clearly showing the effect, the dry sample used for water adsorption is the one obtained from 50 mM nitroxides for labeling, whose spectrum is reported in Fig. 2): ω_{ex} decreased from 4×10^8 to 1×10^8 s^{-1}. The persistence of this signal is accounted for by (i) sharp curvatures due to the flexibility of the fibers, providing regions in which the labels are protected from complete hydration; and (ii) spin–spin interactions among labels that were stronger than the water–label interactions. Both possibilities may affect the hydration process simultaneously.

Shaking the fiber in water to form a dispersion leads to the disappearance of the slow-moving component from the EPR spectrum, which is then only constituted by the two components due to fast-moving radicals in polar and low-polar environments (Fig. 3, top right). These two components were also present in the spectrum of MMVF10 + 10 μL of water, but the relative amounts were different: in the water dispersion the polar component increased and became predominant with respect to the fibers in 10 μL of water, due to complete water hydration.

(2) The spectrum of JM104 after addition of 10 μL of water is constituted by three narrow lines, as usually found for very fast-moving radicals ($\tau_c \approx 1 \times 10^{-11}$ s) in a low-polar environment. JM104 is highly soluble. As shown from the analysis of Fig. 1, the surface was scarcely labeled, but the labels strongly interacted with the water molecules and/or hydrophilic sites at the surface (probably ions, as inferred by the composition reported in Table 1). Water easily interposes among the labels and preferentially interacts with the ions at the surface. The labels, therefore, cease to move and the hydrophobic interactions prevails, also due to the high flexibility of the fibers.

It is interesting to note, from spectral analysis, that the lower the mobility in the dry sample, the higher the amount of labels which localize in low-polar environments. This effect may be related to the presence of ions at the surface and to the preferential hydration of the ionic sites at the surface (also tested by calorimetric measurements; see below). In other words, in the absence of water, the polar groups of the labels are immobilized at the ionic sites of the surface. After water addition, the water molecules preferentially hydrate the ions and hydrophobic interactions may prevail for the labels (due to the aminopropyltrimethoxysilane group and the hydrophobic sites at the surface).

Isotherms and Heat of Adsorption of Water

The MMVF11 of lot 1 exhibited anomalous behavior with water vapor. The adsorption was extremely slow, indicating not mere adsorption but a reaction unexpected for a glass surface. Treatment with hydrochloric acid fully modified the nature of the surface. The slow process disappeared and the amount of water adsorbed per unit surface was higher. The kinetics and heat values were in agreement with those expected for a glass surface (regular curves). This confirms that the surface of MMVF11 from lot 1 is contaminated with substances which are chemically very different from glass. The results from the acid-treated sample were therefore considered typical of the nature of the MMVF11 surface.

The isotherms for the adsorption of water on the MMVFs are reported in Fig. 4, while Table 5 compares the amount of water adsorbed up to 5 Torr on vitreous fibers with that adsorbed on vitreous and crystalline silica (24). When measured at the same equilibrium pressure (e.g., 5 Torr, Table 5), the amount of water

TABLE 5
Amount of Water Adsorbed up to 5 Torr on MMVF10, MMVF11, MMVF21, and Vitreous (Suprasil) and Crystalline Silica (Cristobalite)

	TOT (μmol m^{-2})	REV (μmol m^{-2})	IRR (μmol m^{-2})
MMVF10	51	30	21
MMVF11	46.5	35	11.5
MMVF21	25	16	9
Cristobalite	9.4	8.1	1.3
Suprasil	9.3	8	1.3

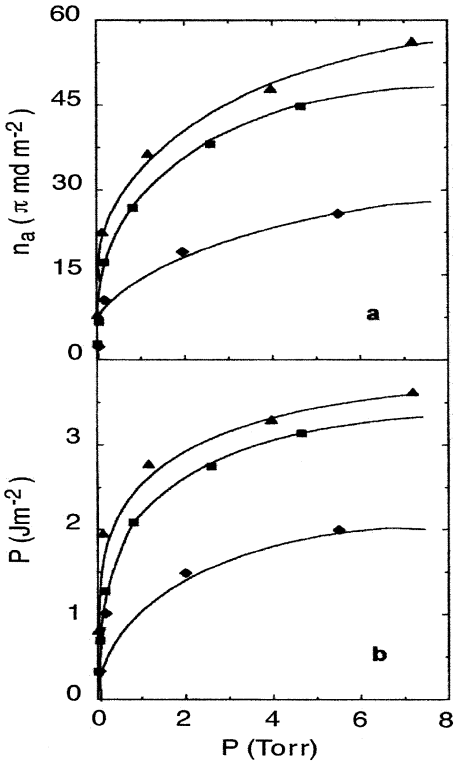

FIG. 4. (a) Volumetric isotherms (n_a vs p) and (b) calorimetric isotherms (Q vs p) for the adsorption of vapor H_2O in the first adsorption run (Ads I) on glass fibers outgassed at 150°C: MMVF10 (triangles), MMVF11 (squares), and MMVF21 (diamonds).

adsorbed per unit surface varies in the sequence

$$\text{MMVF10} > \text{MMVF11} \gg \text{MMVF21} > SiO_2;$$

the differences are related to the different chemical compositions.

The adsorption of water onto a glass surface is a complex matter as water is not only adsorbed on OH but also coordinated by cations. The number of adsorbed water molecules depends on the kind of exposed cations, on how deeply water penetrates the subsurface layers, and on the strength of the metal ion–water bond. Penetration of water into subsurface layers favors dissolution. The rock wool (MMVF21) adsorbs less water than the glass wool (MMVF10 and MMVF11) under the same conditions, for the following reasons:

- glass fibers have more SiOH groups (for H-bonding to water) than rock fibers;
- glass fibers have more metal ions coordinating to water than rock fibers;
- water dissolves more easily onto glass than onto rock fibers.

For all the MMVF fibers, however, the adsorbed amounts are much greater than those on crystalline silicas (25–28). This clearly indicates that the increased adsorption onto glass fibers is mostly related to the presence and abundance of metal cations (for the type of cations, see Table 1).

The analysis of the heat curves and kinetics confirms this result. The available cations and their capability of coordinating to water is higher on the glass than on the rock samples. The greater the water coordination, the easier the solubilization of the fiber. Accordingly, rock wool fibers are less soluble and consequently more biopersistent (28).

If we plot the differential heat values (heat per adsorbed moles) as a function of the equilibrium pressure (this parameter defines the state of hydration of the surface), we obtain a representation of the kind of interaction independent of the actual number of surface sites which adsorb water. Such a diagram is reported in Fig. 5 for the total and the reversible adsorption of water onto MMVF10, MMVF11, and MMVF21. As all points remarkably fall on the same curve, we may infer that the chemical processes taking place at the surfaces of the various vitreous fibers are qualitatively the same.

Interaction of Water with Labeled Surfaces

Modification of the surface properties of the fibers induced by labeling has been studied by measuring the heat of adsorption of water before and after linking of the aminopropyl chain.

The curves obtained for adsorption of water onto the HCl-washed surface of MMVF11 and on the same specimen after functionalization are reported in Fig. 6a as calorimetric isotherms (total heat vs pressure) and in Fig. 6b as differential heat (heat per adsorbed mole) as a function of adsorption. Functionalization does not modify the surface, too deeply; i.e., the surface is still hydrophilic, and the two curves in Fig. 6a are equivalent over a wide range of coverage. This indicates that there is a part of the surface which is not modified by the functionalization. A comparison of the curves in Figs. 6a and 6b reveals the following:

—the adsorption heat is negligible above 1 Torr equilibrium pressure; i.e., once the uncovered surface is saturated, adsorption does not proceed on the covered one and a plateau is attained;

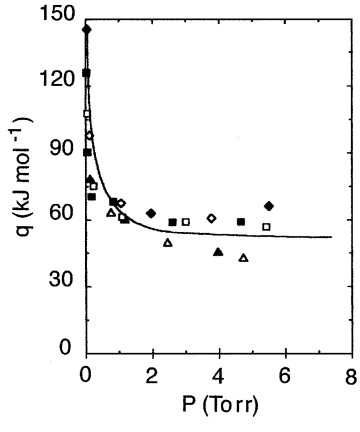

FIG. 5. Differential heat of adsorption (q vs p) of H_2O vapor in the first (Ads I, filled symbols) and second (Ads II, empty symbols) adsorption runs on glass fibers outgassed at 150°C: MMVF10 (triangles), MMVF11 (squares), and MMVF21 (diamonds).

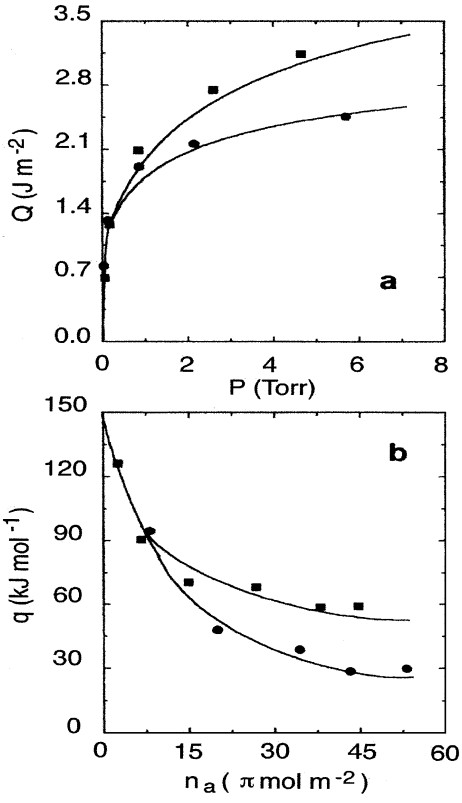

FIG. 6. (a) Calorimetric isotherms (Q vs p) and (b) differential heat (q vs n_a) for H_2O vapor in the first adsorption run (Ads I) on MMVF11 fibers outgassed at 150°C: HCl-washed surface (circles); labeled surface (squares).

—the initial heat on the functionalized surface is low (loss of the most energetic adsorption sites);

—adsorption proceeds on the labeled surface but with a low heat of interaction.

SUMMARY

Surface-bound spin labels, by providing—through computer-aided analysis of the EPR spectra—structural and mobility parameters, are an appropriate tool for the analysis of the local topography of a silica-based surface. They give information on the distribution of the labels in regions that differ in their polarity and interacting ability. The results obtained were consistent with the variation, from one sample to another, of the following characteristics: (a) the presence of ions at the surface; (b) the silica contents; (c) the vicinity of SiOH groups, which are responsible for spin–spin interactions (dipolar or Heisenberg exchange); (d) fiber dimension and morphology of the surfaces; (e) polar and low-polar regions at the surface; (f) water hydration.

The main conclusions on the surface characteristics of the fibers examined are as follows:

(1) The mobility of the labels decreased following interaction with either ions or ionic and polar groups at the surface.

(2) Close interacting sites are easily identified on the basis of spin–spin interactions and strongly and weakly interacting sites may be distinguished (and quantified on the basis of the silica content).

(3) The spin-labeling technique allowed identification of different silicon concentrations and of contaminants at the surface.

(4) The interaction with water reveals substantial heterogeneity in the hydrophilicity of surface sites. Water in contact with labeled fibers first adsorbs in surface regions located far from the label and water molecules approach the label only after a large part of the free surface has been wetted. This indicates that labeling takes place on the least hydrophilic part of the material and that the labels are not easily hydrated, hydrophobic interactions prevailing for labels which locate in low-polar regions.

(5) The reaction of water vapor with vitreous fibers of different compositions reveals that these materials adsorb much more water than any crystalline or amorphous silica, water coordinated to surface cations playing a major role in the overall adsorption. The surface reaction mechanisms are the same on fibers of different compositions, as revealed by the substantial similarity of the interaction energies, but the surface composition affects the extent of adsorption. Glass wool exhibits a much higher adsorption capacity than rock wool under the same experimental conditions.

ACKNOWLEDGMENTS

The authors thank the Joint European Medical Research Board (JEMRB) for the financial support. The authors are also indebted to Dr. L. Mollo for running some of the EPR spectra reported.

REFERENCES

1. Warheit, D. B., "Fiber Toxicology." Academic Press, New York, 1993.
2. Davis, J. M. G., and Jaurand, M. C., *in* "Cellular and Molecular Effects of Mineral and Synthetic Dusts and Fibers," NATO ASI Series, Vol. H 85, p. 425. Springer-Verlag, Berlin/New York, 1994.
3. Kane, A. B., Boffetta, P., Saracci, R., and Wilbourn, J. D., "Mechanisms of Fiber Carcinogenesis," IARC Scientific Publication 140. International Agency for Research on Cancer, Lyon, 1996.
4. Guthrie, G. D., and Mossman, B. T., "Health Effects of Mineral Dusts," Reviews in Mineralogy, Vol. 28. Mineral. Soc. of America, Washington, D.C., 1993.
5. Fubini, B., *in* "Fiber Toxicology" (D. B. Warheit, Ed.), p. 229. Academic Press, New York, 1993.
6. Fubini, B., *Environ. Health Perspect.* **105,** 1013 (1997).
7. Fubini, B., Giamello, E., Mollo, L., Zanetti, G., Eborn, S. K., and Aust, A. E., *Res. Chem. Intermed.*, **25,** 95 (1999).
8. Fubini, B., *in* "Health Effect of Silica in the Surface Properties of Silicas" (J. P. Legrand, Ed.), p. 415. Wiley Chichester, 1997.
9. Donaldson, K., and Borm, J. A., *Ann. Occup. Hyg.* **47,** 287 (1998).
10. Berliner, L. J., "Spin Labeling. Theory and Applications," Vol. 1. Academic Press, New York, 1976; Vol. 2. Academic Press, New York, 1979.
11. Berliner, L. J., and Reuben, J., "Biological Magnetic Resonance. Spin Labeling, Theory and Applications," Vol. 8. Plenum, New York, 1989.
12. Mollo, L., Levresse, V., Ottaviani, M. F., Ellouk-Achard, S., Jaurand, M. C., and Fubini, B., *Environ. Health Perspect.* **105,** 1031 (1997).
13. Ottaviani, M. F., Mollo, L., and Fubini, B., *J. Colloid Interface Sci.* **191,** 154 (1997).
14. (a) Axten, C. W., Bauer, J. F., Boymel, P. M., Copham, J. D., Cunningham, R. N., Kamstrup, O., Koenig, A., Konzen, J. L., Ohberg, I., Roe, C., Sacks, J., and Wolf, W. (TIMA Nomenclature Committee members) "Man-Made

Vitreous Fibers. Nomenclature, Chemistry and Physical Properties" (W. Eastes and Owens–Corning Fiberglas, Eds.), Stamford, CT, 1991. (b) Bunn, W. B., Bender, J. R., Hersterberg, T. W., Chase, G. R., and Konzen, J. L., *J. Occup. Med.* **35,** 101 (1994).
15. (a) Hommel, H., Legrand, A. P., Ben Ouada, H., Bouchriha, B., Balard, H., and Papirer, E., *Polymer* **33,** 181 (1992). (b) Ben Ouada, H., Hommel, H., and Legrand, A. P., *J. Chem. Soc. Faraday Trans.* **84,** 3865 (1988).
16. Malcolm, T., Gorse, J., and Kooser, R. G., *J. High Resolut. Chromatogr. Chromatogr. Commun.* **11,** 416 (1988).
17. Hall, L. D., and Waterton, J. C., *J. Am. Chem. Soc.* **101,** 3697 (1979).
18. Fubini, B., *Thermochim. Acta* **135,** 19 (1988).
19. Schneider, D. J., and Freed, J. H., *in* "Biological Magnetic Resonance. Spin Labeling. Theory and Applications." (L. J. Berliner and J. Reuben, Eds.), Vol. 8, p. 1. Plenum, New York, 1989.
20. Plachy, W., and Kivelson D., *J. Chem. Phys.* **47,** 3312 (1967).
21. Aizawa, M., Komatsu, T., and Nakagawa, T., *Bull. Chem. Soc. Jpn.* **52,** 980 (1979); **53,** 975 (1980).
22. Sackmann, E., and Träuble, T., *J. Am. Chem. Soc.* **94,** 4482, 4492, 4499 (1972).
23. Martini, G., Bindi, M., Ottaviani, M. F., and Romanelli, M., *J. Colloid Interface Sci.* **108,** 140 (1985).
24. Bolis, V., and Fubini, B., *in* "New Compounds Materials" (E., Daolto, E. Tondello, and P. A. Vigato, Eds.), Vol. 5, 1995.
25. Bolis, V., Fubini, B., Marchese, L., Martra, G., and Costa, D., *J. Chem. Soc. Faraday Trans.* **87,** 497 (1991).
26. Fubini, B., Bolis, V., Cavenago, A., Garrone, E., and Ugliengo, P., *J. Chem. Soc. Faraday Trans.* **88,** 277 (1992).
27. Fubini, B., Bolis, V., Cavenago, A., Garrone, E., and Ugliengo, P., *Langmuir* **9,** 2712 (1993).
28. Hesterberg, T. W., Miller, W. C., Musselman, R. P., Kamstrup, O., Hamilton, R. D., and Thevenaz, P., *Fundam. Appl. Toxicol.* **29,** 267 (1996).